LA-8342

c. 3

Cross Sections for Neutron-Induced, Neutron-Producing Reactions in ^{6}Li and ^{7}Li at 5.96 and 9.83 MeV

LOS ALAMOS SCIENTIFIC LABORATORY
Post Office Box 1663 Los Alamos, New Mexico 87545

This work was supported by the US Department of Energy, Office of Basic Energy Sciences.

Edited by Martha Lee DeLanoy

Photocomposition by Chris West

UNITED STATES
DEPARTMENT OF ENERGY
CONTRACT W-7405-ENG. 36

LA-8342

UC-34c
Issued: October 1980

Cross Sections for Neutron-Induced, Neutron-Producing Reactions in ^{6}Li and ^{7}Li at 5.96 and 9.83 MeV

P. W. Lisowski
G. F. Auchampaugh
D. M. Drake
M. Drosg*
G. Haouat**
N. W. Hill†
L. Nilsson††

*Short-Term Visiting Staff Member. University of Vienna, Vienna, AUSTRIA.
**Consultant. Centre d'Etudes de Bruyères-le-Châtel, FRANCE.
†Visiting Scientist. Oak Ridge National Laboratory, Oak Ridge, TN 37830.
††Short-Term Visiting Staff Member. Tandem Accelerator Laboratory, Uppsala, SWEDEN.

CROSS SECTIONS FOR NEUTRON-INDUCED, NEUTRON-PRODUCING REACTIONS IN ^{6}Li AND ^{7}Li AT 5.96 AND 9.83 MeV

by

P. W. Lisowski, G. F. Auchampaugh, D. M. Drake, M. Drosg, G. Haouat, N. W. Hill, and L. Nilsson

ABSTRACT

Using the time-of-flight technique, we have measured the ^{6}Li and ^{7}Li neutron emission spectra at incidental neutron energies of 5.96 and 9.83 MeV and at 10 angles from 25° to 144°. This report presents differential elastic and inelastic cross sections as well as continuum cross sections that result from three-body breakup and inelastic scattering from unresolved states.

I. INTRODUCTION

Cross sections for neutron-induced reactions in several light nuclei are important to the studies of neutronics and tritium breeding in possible fusion-reactor designs. Lithium isotopes are of particular interest as constituents in the blanket material of fusion reactors because of the tritium produced by the reactions $^{6}Li(n,t)^{4}He$ (Q = +4.784 MeV) and $^{7}Li(n,t)n^{4}He$ (Q = −2.467 MeV). Furthermore, several neutron-induced reactions in the lithium isotopes emit two neutrons in the exit channel and thus support the neutron economy of the fusion-reactor system.

This report presents measurements of the angular and energy distribution of outgoing neutrons produced by ^{6}Li + n and ^{7}Li + n interactions at 5.96 and 9.83 MeV. The outgoing neutrons are produced in a variety of reactions. The resultant emission spectra, which contain both peaks and continuum, are complicated. The reactions are described in Batchelor and Towle.[1]

We analyzed the definable peaks of the time-of-flight (TOF) spectra and placed the rest of the emission spectra in a continuum. For ^{6}Li + n, we determined the elastic-scattering and inelastic-scattering cross sections to the 2.185-, 3.56-, and 4.31-MeV states. For ^{7}Li + n, we obtained cross sections for the sum of the elastic scattering and unresolved inelastic scattering to the 0.48-MeV excited state, as well as cross sections for the inelastic scattering to the 4.63-MeV second excited state and to the 6.7-MeV third excited state.

We measured neutron TOF spectra at 10 angles between 25° and 144° at incident neutron energies of 5.96 and 9.83 MeV. Cross sections at each angle were determined as a function of emergent neutron energy.

Recently, angular-distribution measurements of elastic cross sections and some discrete inelastic cross sections have been completed for both lithium isotopes. Knox, White, and Lane[2] have measured the 4- to 7.5-MeV energy range, and a group at Triangle Universities Nuclear Laboratory[3] has measured the

7.0- to 13.9-MeV energy range. Earlier measurements than those in Ref. 1 were made by Rosen and Stewart[4] from 5 to 14 MeV; by Cookson, Dandy, and Hopkins[5] at 10 MeV; and by Hopkins, Drake, and Conde[6] from 4.8 to 7.5 MeV. Because neutrons scattered by the 0.478-MeV first excited state of ^{7}Li are difficult to resolve from elastically scattered neutrons, the cross sections for this state have been measured at other laboratories by detecting the 0.478-MeV gamma ray. In particular, Batchelor and Towle,[1] Presser and Bass,[7] Morgan,[8] and an Oak Ridge National Laboratory group[9] have reported such data.

Thus, the elastic-scattering and discrete inelastic-scattering cross sections (to the first and second excited states) for lithium are reasonably well-known. However, inelastic cross-section data are rare, and double-differential data of the type reported here are practically nonexistent.

II. EXPERIMENTAL PROCEDURE

Because our experimental method is described in detail in Ref. 10, only information pertinent to the present work is included here. The experimental arrangement is shown in Fig. 1.

The H(t,n)^{3}He reaction provided the intense monoenergetic source of neutrons for our studies. Approximately 500 nA of a pulsed tritium beam from the Los Alamos Scientific Laboratory (LASL) tandem Van de Graaff bombarded 3 atm of hydrogen gas in a 30-mm-long by 10-mm-diam cell. The cell had an entrance foil of 5.2-mg/cm^2 molybdenum and a gold beam stop. The neutron beam struck an isotopically enriched ^{6}Li or ^{7}Li metal sample in a thin-aluminum holder. An empty aluminum holder of identical dimensions was used to measure the background, as described below. Each cylindrical sample was positioned with the symmetry axis vertical and at a source-to-sample distance of approximately 135 mm. Table I summarizes the sample characteristics.

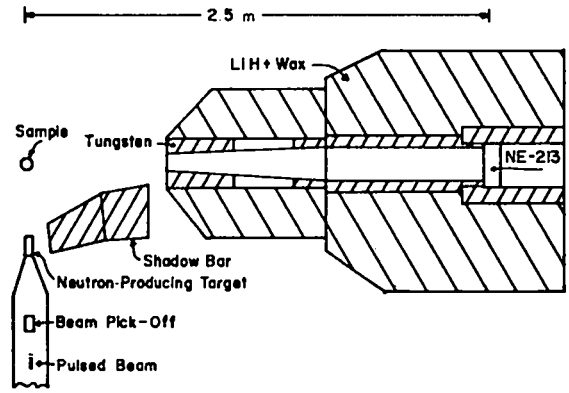

Fig. 1.
Experimental arrangement for the neutron TOF measurements.

TABLE I

SAMPLE CHARACTERISTICS

Sample	Weight (g)	Diameter (cm)	Height (cm)	Isotopic Purity
^{6}Li	3.49	1.98	2.70	0.9905
^{7}Li	4.05	1.98	2.70	0.9996
Polyethylene	2.94	1.27	2.54	
Carbon	2.85	1.27	2.54	
Empty aluminum holder	1.4	1.98	2.70	

Outgoing neutrons were detected by an NE-213 liquid scintillator* that is within a massive shield and is 2.53 m from the sample. To improve light-collection efficiency, an RCA-8854 photomultiplier tube** was coupled directly to the liquid scintillator. A large tungsten shadow bar with an effective length of 240 mm shielded the neutron detector from the target's direct gamma rays and neutrons. The reaction angle was changed by rotating the neutron detector and its shield about the center of the sample. The detector bias was set in the pulse-height minimum below the 59-keV ^{241}Am gamma ray to give a neutron energy bias of about 300 keV.

A standard pulse-shape discrimination (PSD) circuit[11] was used to separate neutron and gamma-ray events. TOF information was obtained from an EG&G TDC-100 time digitizer† set to record in 0.5-ns time bins. To permit detailed scrutiny of the data after the experiment, the PSD, the TOF, and the recoil-proton pulse height were stored in a three-parameter event-by-event mode on magnetic tape by an SDS-930 computer.†† On-line spectra, collected by using computer-generated gates on each of the three parameters, enabled us to monitor and examine the data as they were accumulated.

A monitor detector consisting of a small plastic scintillator mounted on an RCA-8575 photomultiplier tube** was positioned in the reaction plane at an angle of about 15°, approximately 8 m from the neutron source. This detector, which measured neutrons from the source by time of flight, was used to normalize the measurements. Serving as a secondary monitor was a separate current-integrating system (for the triton beam) that provided the normalization for background measurements with the source gas removed. The neutron monitor and current integrator agreed to within ~1% for all gas-in data.

To account for sources of background neutrons, the data were taken in the fourfold measurement sequence that is described in Ref. 10 and summarized below. After being normalized to the monitor detector count or to the integrated triton-beam current, the TOF spectrum $Y(E;E',\theta)$, resulting from neutrons of energy E incident on lithium, was formed from the following four measured spectra.

*Nuclear Enterprises, Inc., San Carlos, CA 94070.
**RCA, New York, N. Y. 10020.
†EG&G, Ortec, Inc., Oak Ridge, TN 37830.
††Scientific Data Systems, Santa Monica, CA 90406.

$$Y(E;E',\theta) = Y(\text{sample in, gas in}) - Y(\text{sample out, gas in}) - Y(\text{sample in, gas out}) + Y(\text{sample out, gas out}) ,$$

where Y(A,B) represents a spectrum measured under conditions specified by A and B, and E' and θ indicate the dependence on outgoing energy and angle, respectively. The expressions "gas in" and "gas out" refer to the condition of the source reaction-gas cell. Figure 2 shows a set of four TOF spectra and the resulting n + ^{7}Li spectrum for incident 9.83-MeV neutrons at a 60° laboratory angle (θ_{lab}).

At each energy, a series of auxiliary mesurements was taken with polyethylene and carbon scatterers providing cross-section normalization to well-known H(n,n)H scattering. For these data, only source gas-in spectra were taken. The carbon spectrum was subtracted from the polyethylene spectrum to give only the n-p scattering (Fig. 3).

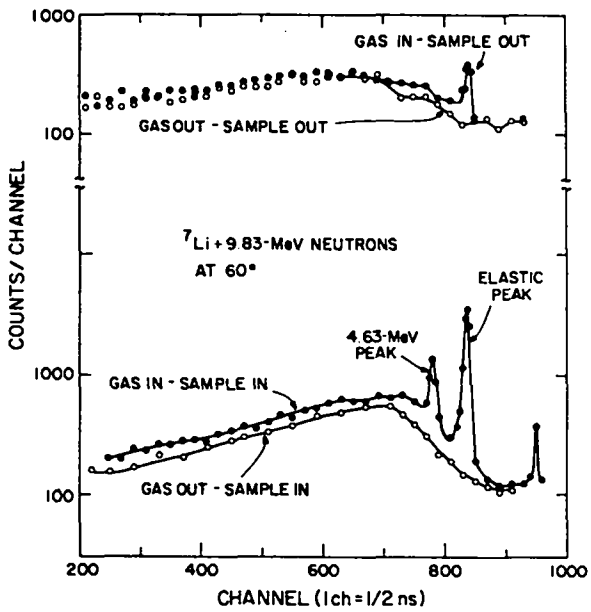

Fig. 2.
Raw TOF spectra at 60° for each of the four target-sample configurations. The bottom two curves show spectra with the ^{7}Li sample in place when the target cell was filled with gas and when it was empty. The upper two curves show similar spectra with the empty aluminum sample holder replacing the ^{7}Li sample.

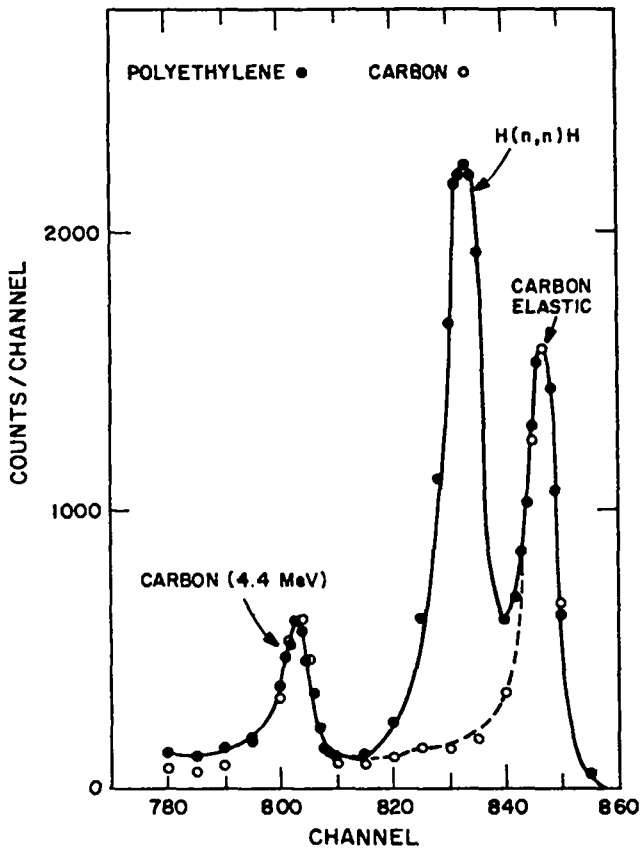

Fig. 3.
TOF spectra for neutrons scattered from samples of polyethylene and carbon at 25° and 9.83 MeV.

III. DATA REDUCTION

The double-differential cross sections calculated according to the FORTRAN code described in Ref. 10, except that the following expression, which is equivalent to Eq. (3) in Ref. 10, was used for the evaluation.

$$\frac{d^2\sigma}{d\Omega dE'} = \frac{Y(E;E',\theta)}{Y_H(E_H,\theta_H)} \frac{m_H(E_H,\Omega_H)}{m_s(E;E',\Omega)} \frac{\varepsilon(E_H)}{\varepsilon(E')} \times \frac{n_H}{n_s} \sigma_H(E_H,\theta_H) \frac{F_H}{F_s} ,$$

where

$Y(E;E',\theta)$ is the normalized, background-subtracted, and deadtime-corrected yield per unit energy resulting from incident neutron energy E and outgoing energy E' at angle θ;

$Y_H(E_H,\theta_H)$ is the normalized, background-subtracted, and deadtime-corrected yield at incident energy E_H and angle θ_H obtained by summing the n-p scattering peak;

$m_s(E;E',\Omega)$ is the correction for multiple scattering of neutrons of energy E into neutrons of energy E' and solid angle Ω for the lithium sample;

$m_H(E_H,\Omega_H)$ is the correction for multiple scattering of neutrons of energy E_H into solid angle Ω_H integrated over the hydrogen scattering peak;

$\varepsilon(E_H)$ and $\varepsilon(E')$ are the relative efficiencies for the detection of neutrons of energy E_H from the polyethylene and of neutrons of energy E' from the lithium samples, respectively;

n_H and n_s are the numbers of hydrogen nuclei in the polyethlene and lithium nuclei in each sample;

$\sigma_H(E_H,\theta_H)$ is the differential cross section for the scattering of neutrons of energy E_H from hydrogen at angle θ_H; and

F_H and F_s are the fluence factors to correct for the effect of different-sized polyethylene and lithium samples (see Table I).

The Monte Carlo computer code written to evaluate F_H and F_s for our source reaction and geometry uses the equations of Ref. 12. For our conditions, F_H/F_s is 1.000 ± 0.001 at each energy.

The hydrogen differential cross-section values $\sigma_H(E_H,\theta_H)$ were computed from Yale phase shifts,[13] which appear to fit experimental data better than Lawrence Livermore Laboratory phase shifts or Gammel's formula.[14]

We measured the relative efficiency of our detector from 0.3 to 16 MeV. Because of inconsistencies when using the data of the Liskien and Paulsen[15] evaluation as reference values, the data of Drosg[16] were used for $^2H(d,n)^3He$ cross sections. The relative efficiency curve (Fig 4.) is the curve described in Ref. 17.

Multiple scattering corrections came from neutron transport calculations performed by the LASL Monte Carlo code MCNP.[18] The details of the calculations are discussed in Ref. 10. In our experiment, the corrections ranging from 0.85 to 1.15 were close to 1.1 over most of the energy range.

IV. ERROR ANALYSIS

In addition to statistical uncertainties of the data, we have added the following sources of errors to the statistical standard deviation in quadrature.

Detector efficiency	3% for $0.5 \leq E_n \leq 10$ MeV 10% for $E_n \leq 0.5$ MeV
Multiple scattering	half the value of the correction
Normalization of raw spectra	1% difference between runs
Extrapolations	50% below 0.3 MeV 25% under inelastic peaks

V. RESULTS

A. Cross Sections for ^6Li + 5.96-MeV Neutrons

The angular distribution of the elastic-scattering cross sections for ^6Li bombarded by 5.96-MeV neutrons (Fig. 5* and Appendix Table A-I) agrees well with previously published results[2] at nearby energies. The inelastic-scattering differential cross section of the 2.18-MeV excited state also is shown in Fig. 5. Integrations over angle for the two distributions give 1308 ± 82 and 171 ± 14 mb, respectively (Table A-II). These values also agree reasonably well with earlier results.[1,2,6] The continuum cross section (Table A-III) has been integrated over energy and angle with extrapolations from about 0.3 to 0.0 MeV on the low-energy side and under the 2.18-MeV peak on the high-energy side. When we add the angle-integrated continuum cross section of 496 ± 64 mb to the elastic, inelastic, and partial cross sections of 17 mb (Ref. 19) and 66 mb (Ref. 20) for (n,p) and (n,α) reactions, we get a total cross section of 2058 ± 104 mb. The total cross section in Ref. 21 is about 2000 mb.

In Fig. 6, a small peak corresponding to the excitation of the 3.56-MeV second excited state appears at backward angles where the continuum is small. We

*In Fig. 5 and subsequent figures in which elastic angular distributions are shown, σ_w represents the lower limit of the elastic zero-degree cross section.

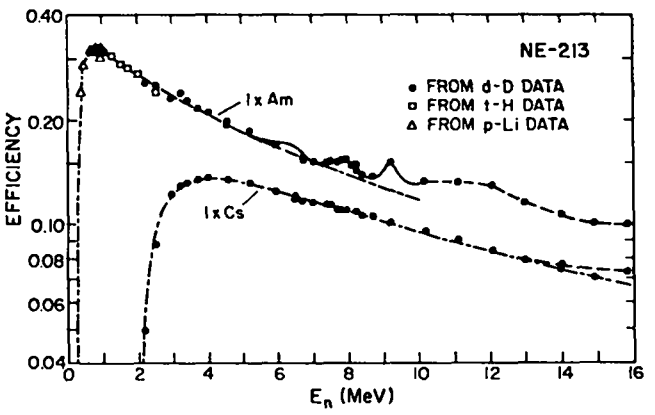

Fig. 4.
Relative efficiency curves (as a function of incident neutron energy E_n) for the detector used in this experiment. The upper curve corresponds to a neutron bias of 300 keV and is designated 1 x Am because this bias is set using the ^{241}Am 59-keV gamma ray. The bumps in this curve can be attributed to neutron-carbon interactions in the NE-213 scintillator. The lower curve, corresponding to a neutron bias of about 2 MeV, is designated 1 x Cs because the bias is set at the half height of the Compton edge for the ^{137}Cs 662-keV gamma ray.

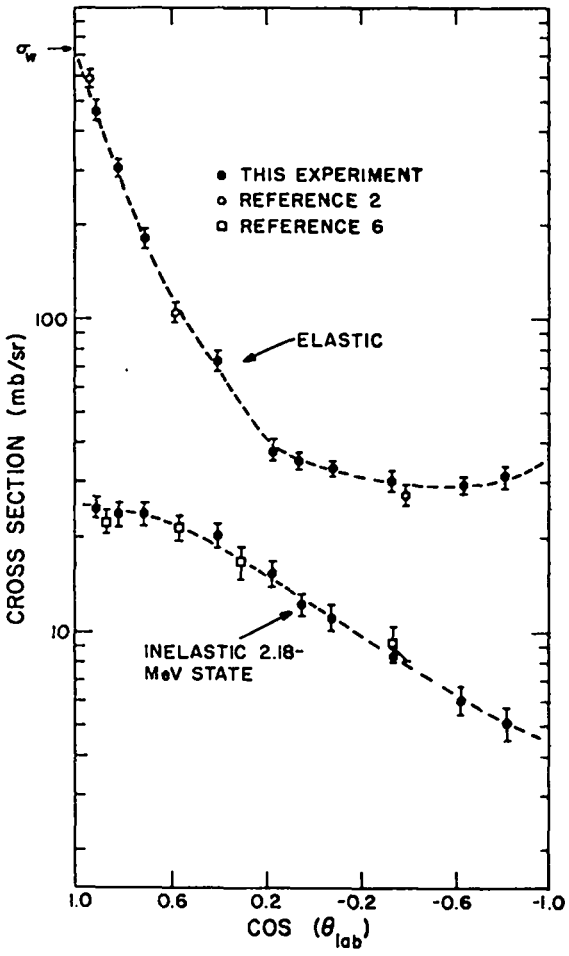

Fig. 5.
Angular distributions of the elastic and inelastic (E^* = 2.18 MeV) scattering cross sections for ^{6}Li bombarded by 5.96-MeV neutrons. The dashed line through the elastic distribution was calculated from the Legendre polynomials in Table A-IV.

have included this peak in the continuum integral although cross sections of 0.8 ± 0.5, 0.8 ± 0.4, and 0.7 +0.5/-0.3 mb/sr can be extracted for the angles of 95°, 110°, and 125°, respectively. These values are consistent with the 6.5-mb (n,n'γ) cross-section value of Presser, Bass, and Kruger,[22] who measured the gamma-ray decay of this T = 1 state.

B. Cross Sections for ^{7}Li + 5.96-MeV Neutrons

We have measured the differential elastic + 0.48-MeV state cross sections for 5.96-MeV neutrons on ^{7}Li at 10 angles (Table A-I); however, because the energy of neutrons scattered from the 4.63-MeV excited state at backward angles is close to the bias, we cannot estimate reliable cross sections beyond 60° for that state. Two typical spectra are shown at the bottom of Fig. 6. The differential elastic + 0.48-MeV cross sections, shown in Fig. 7, agree well with the cross sections measured by Knox, White, and Lane.[2] When the angle-integrated elastic + 0.48-MeV excited-state cross sections of 1715 ± 108 mb are added to the 127 ± 50 mb estimated for the 4.63-MeV state and the 249 ± 35 mb for the angle- and energy-integrated continuum (Table A-II), they give a total cross section of 2091 ± 124 mb. The total cross section in Ref. 21 is 2100 mb.

C. Cross Sections for ^{6}Li + 9.83-MeV Neutrons

Neutron-emission spectra for two angles are shown in Fig. 8 for ^{6}Li + 9.83-MeV neutrons. The angular distributions of the elastically scattered

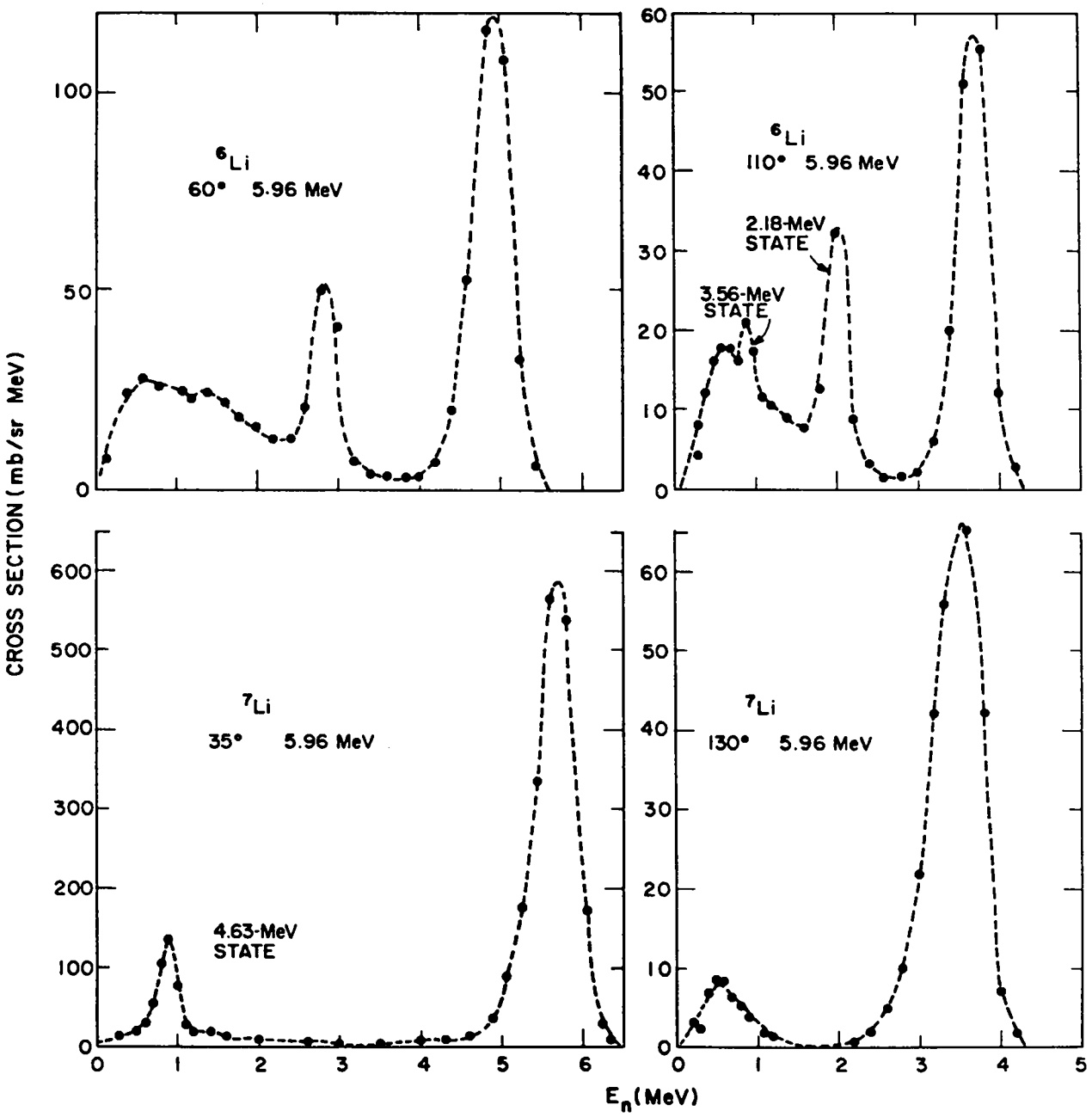

Fig. 6.
Typical emission cross sections for 5.96-MeV neutron bombardment of ^{6}Li and ^{7}Li.

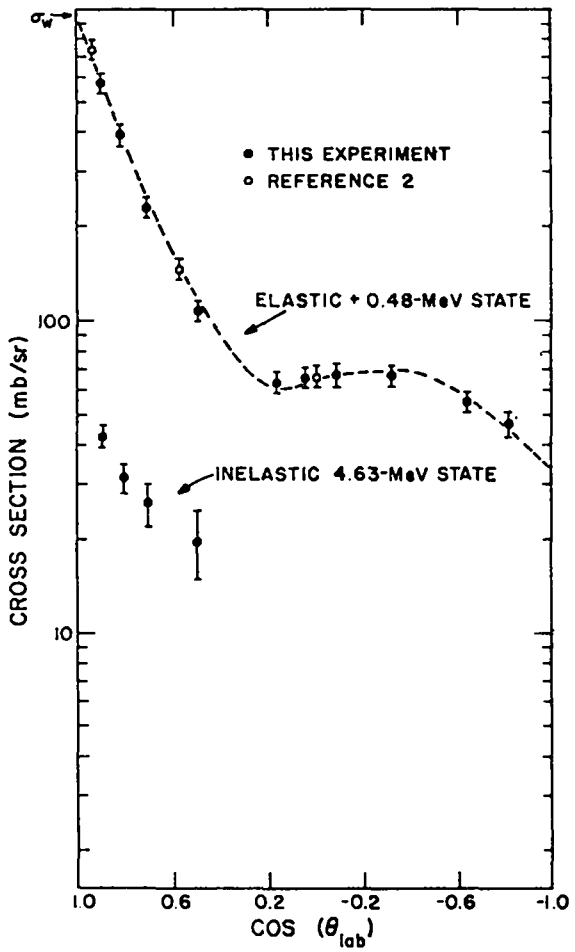

Fig. 7.
Angular distributions of the elastic + 0.48-MeV state and the inelastic (E^* = 4.63 MeV) scattering cross sections for ^{7}Li + 5.96-MeV neutrons. The dashed line through the elastic distribution was calculated from the Legendre polynomials in Table A-IV.

neutrons are shown in Fig. 9 (Table A-I) with previously published data.[2,5] The angle-integrated cross section for the elastic state, 1044 ± 85 mb (Table A-II), agrees well with both 1030 ± 100 mb in Ref. 3 and 1029 ± 30 mb in Ref. 5. The inelastic angular-distribution cross section for the 2.18-MeV state also is shown in Fig. 9. The angle-integrated cross section for this state, 121 ± 15 mb, agrees well with the 107 ± 30 mb and 107 ± 3 mb in Refs. 3 and 5. Angle and energy integration of the continuum distribution gives 472 ± 60 mb for the total continuum cross section.

Differential cross sections for the 4.31-MeV excited state, estimated from the emission spectra, are listed in Table A-I. The errors associated with these cross sectons are large because the continuum cross section under the peak, which also must be estimated, may contain small, but not apparent, contributions from the 3.56- and 5.37-MeV excited states. Both the differential and angle-integrated cross sections for the 4.31-MeV state are included in the continuum.

We estimate a total neutron cross section of 1044 (elastic) + 121 (2.18-MeV state) + 472 (continuum) + 11 (n,p) [Ref. 19] + 42 (n,αt) [Ref. 20] − 33 (n,2n) [Ref. 20] = 1657 ± 110 mb, a value that agrees well with the total cross section value of 1615 ± 40 mb in Ref. 21.

D. Cross Sections for ^{7}Li + 9.83-MeV Neutrons

Neutron-emission spectra for two angles are shown in Fig. 8 for ^{7}Li + 9.83-MeV neutrons. The angular distribution of the sum of the elastic and inelastic 0.48-MeV state is shown in Fig. 10 (Table A-I) with previously published data.[3,5] The angle-integrated cross section for the elastic + 0.48-MeV state, 1344 ± 107 mb (Table A-II), agrees well with 1268 ± 190 mb (Ref. 5) and 1357 ± 40 mb (Ref. 3).

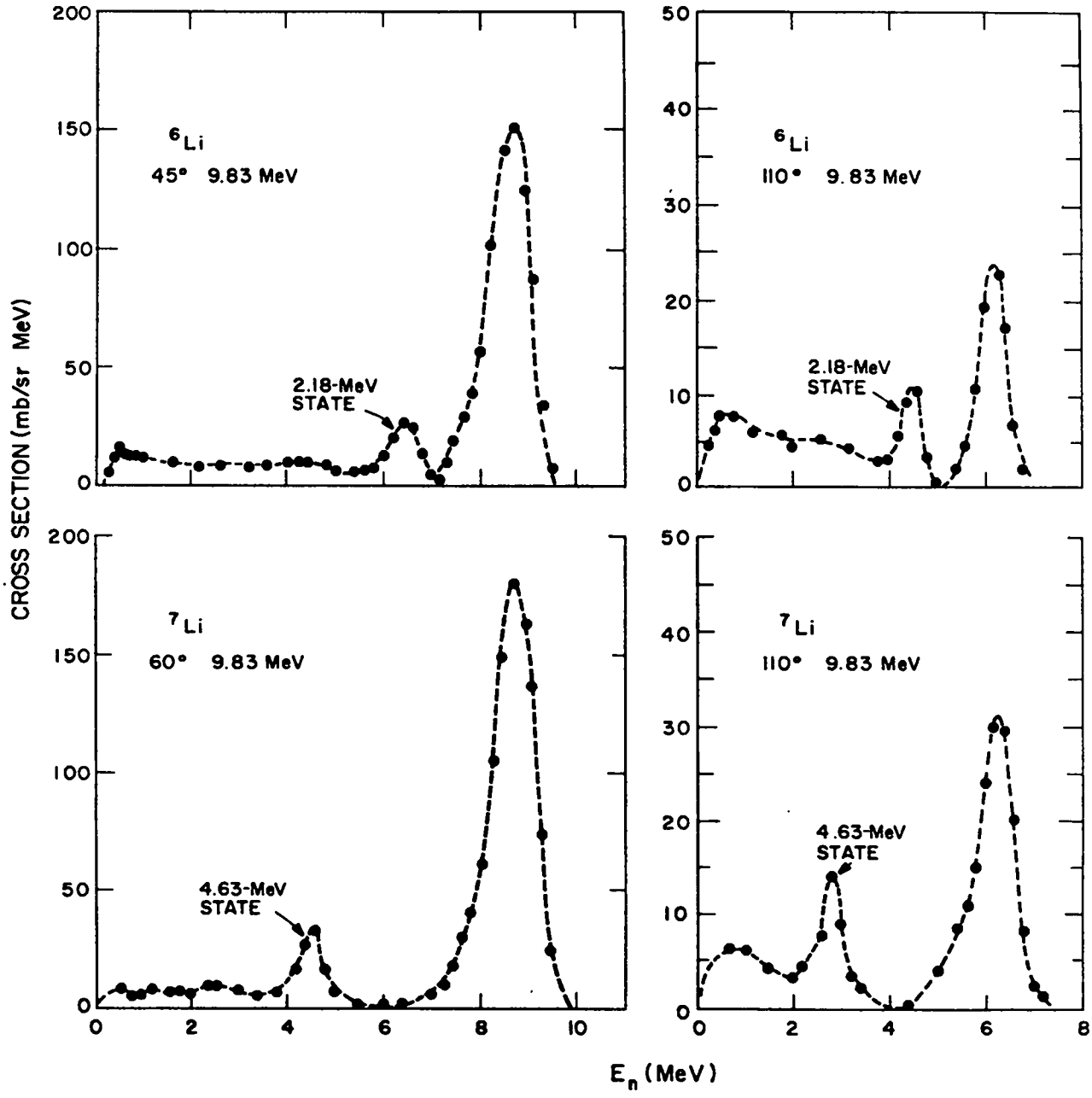

Fig. 8.
Typical emission cross sections for 9.83-MeV neutron bombardment of ^{6}Li and ^{7}Li.

Angular distribution for neutrons scattered by the 4.63-MeV state also is shown in Fig. 10 with representative points from Refs. 3 and 5. The angle-integrated cross section for this state, 127 ± 15 mb, agrees well with the 135 ± 27 mb in Ref. 5, but is lower than the 185 ± 6 mb quoted in Ref. 3. A broad peak corresponding to excitation of the 6.7-MeV state appears in the emission spectra. The angular distribution for this state is in Table A-I, but because the uncertainties associated with the peak are so large, we have included it in the continuum angle and energy integral, which equals 235 ± 35 mb. From the above cross sections, we estimate a total neutron cross section of 1344 (elastic) + 127 (4.63-MeV state) + 235 (continuum) − 27 (n,2n) [Ref. 22] + 10 (n,d) [Ref. 23] = 1689 ± 111 mb, a value that agrees well the the total cross section value of 1680 ± 25 mb in Ref. 21.

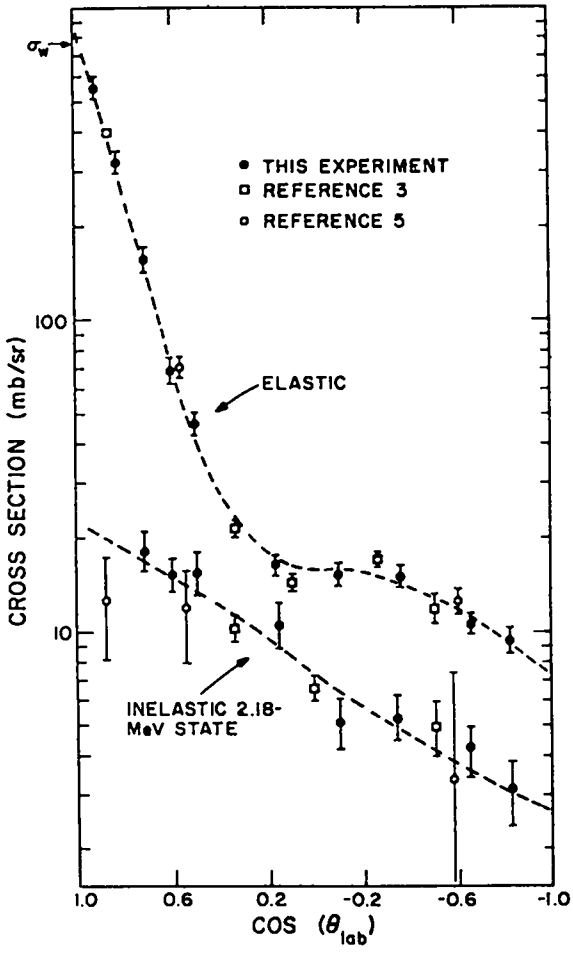

Fig. 9.
Angular distributions of the elastic and inelastic (E^* = 2.18 MeV) scattering cross sections for ^6Li bombarded by 9.83-MeV neutrons. The dashed line through the elastic distribution was calculated from the Legendre polynomials in Table A-IV.

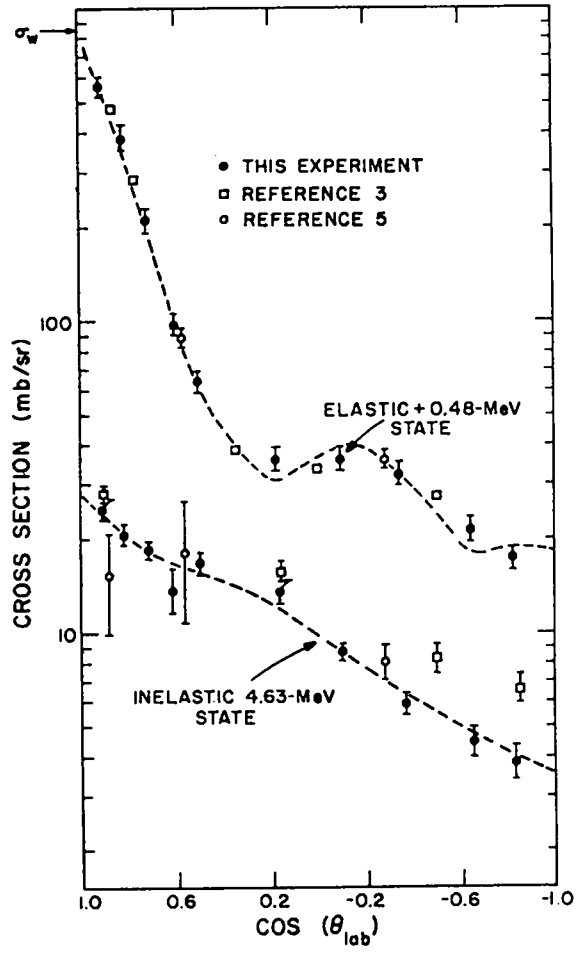

Fig. 10.
Angular distributions of elastic + 0.48-MeV state and the inelastic (E^* = 4.6 MeV) scattering cross sections for ^7Li + 9.83-MeV neutrons. The dashed line through the elastic distribution was calculated from the Legendre polynomials in Table A-IV.

REFERENCES

1. R. Batchelor and J. H. Towle, "The Interactions of Neutrons with Li^6 and Li^7 Between 1.5 and 7.5 MeV," Nucl. Phys. **47,** 385-407 (1963).

2. H. D. Knox, R. M. White, and R. O. Lane, "Differential Neutron Scattering Cross Sections of Lithium-6 and Lithium-7 for Neutrons of 4 to 7.5 MeV Energy", Nucl. Sci. Eng. **69,** 223-230 (1979).

3. H. H. Hogue, P. L. von Behren, D. W. Glasgow, S. G. Glendinning, P. W. Lisowski, C. E. Nelson, F. O. Purser, W. Tornow, C. R. Gould, and L. W. Seagondollar, "Elastic and Inelastic Scattering of 7- to 14-MeV Neutrons from Lithium-6 and Lithium-7," Nucl. Sci. Eng. **69,** 22-29 (1979).

4. L. Rosen and L. Stewart, "Neutron-Induced Disintegration of Li^6 and Li^7," Phys. Rev. **126,** 1150-1151 (1962).

5. J. A. Cookson, D. Dandy, and J. C. Hopkins, "Scattering of 10 MeV Neutrons by ^{6}Li and ^{7}Li," Nucl. Phys. A **91,** 273-291 (1967).

6. J. C. Hopkins, D. M. Drake, and H. Conde, "Elastic and Inelastic Scattering of Fast Neutrons from ^{6}Li and ^{7}Li," Nucl. Phys. A **107,** 139-152 (1968).

7. G. Presser and R. Bass, "Reactions ^{7}Li + n, ^{7}Li + p and Excited States of the A = 8 System," Nucl. Phys. A **182,** 321-341 (1972).

8. G. L. Morgan, "Cross Sections for the ^{7}Li(n,xγ) and ^{7}Li(n,n'α) Reactions Between 1 and 20 MeV," Oak Ridge National Laboratory report ORNL-TM-6247 (March 1978).

9. J. K. Dickens, G. L. Morgan, G. T. Chapman, T. A. Love, E. Newman, and F. G. Perey, "Cross Sections for Gamma-Ray Production by Fast Neutrons for 22 Elements Between Z = 3 and Z = 82," Nucl. Sci. Eng. **62,** 515-531 (1977).

10. D. M. Drake, G. F. Auchampaugh, E. D. Arthur, C. E. Ragan, and P. G. Young, "Double-Differential Beryllium Neutron Cross Sections at Incident Neutron Energies of 5.9, 10.1, and 14.2 MeV," Nucl. Sci. Eng. **63,** 401-412 (1977).

11. T. K. Alexander and F. S. Goulding, "An Amplitude-Insensitive System That Disguishes Pulses of Different Shapes," Nucl. Instrum. Methods **13,** 244-246 (1961).

12. D. E. Velkley, J. D. Brandenberger, D. W. Glasgow, and M. T. McEllistrem, "Sample-Size Effects in Neutron Scattering Studied with Analytic and Monte Carlo Methods," Nucl. Instrum. Methods **129,** 231-239 (1975).

13. J. C. Hopkins and G. Breit, "The ^{1}H(n,n)^{1}H Scattering Observables Required for High-Precision Fast-Neuton Measurements," Nucl. Data, Sect. A **9,** 137-145 (1971).

14. M. Drosg and D. M. Drake, "180 Degree n-p Cross Sections for Fast Neutron Measurements with Counter Telescopes," Nucl. Instrum. Methods **160,** 143-145 (1979).

15. H. Liskien and A. Paulsen, "Neutron Production Cross Sections and Energies for the Reactions T(p,n)^{3}He, D(d,n)^{3}He, and T(d,n)^{4}He," Nucl. Data Tables **11,** 569-619 (1973).

16. M. Drosg, "Unified Absolute Differential Cross Sections for Neutron Production by the Hydrogen Isotopes for Charged-Particle Energies Between 6 and 17 MeV," Nucl. Sci. Eng. **67,** 190-220 (1978).

17. M. Drosg, D. M. Drake, and P. W. Lisowski, "The Contribution of Carbon Interactions to the Neutron Counting Efficiency of Organic Scintillators," Los Alamos Scientific Laboratory report LA-7987-MS (January 1980).

18. LASL Group X-6, "MCNP - A General Monte Carlo Code for Neutron and Photon Transport," Los Alamos Scientific Laboratory report LA-7396-M, Rev. (November 1979).

19. J. F. Barry, "The Cross Section of the Reaction ^{6}Li(n,p)^{6}He in the Neutron Energy Range 3.5 to 14.8 MeV," J. Nucl. Energy, Parts A/B: **17**, 273-275 (1963).

20. J. R. Stehm, M. D. Goldberg, B. A. Magurno, and R. Wiener-Chasman, "Neutron Cross Sections," Brookhaven National Laboratory report BNL-325 (May 1964).

21. D. G. Foster, Jr., and D. W. Glasgow, "Neutron Total Cross Sections 2.5-15 MeV. I. Experimental," Phys. Rev. C: **3**, 576-603 (1971).

22. G. Presser, R. Bass, and K. Kruger, "The Reactions ^{6}Li(n,p)^{6}He(0) and ^{6}Li(n,n')^{6}Li(3.56)," Nucl. Phys. A **131**, 679-697 (1969).

23. M. E. Battat, D. J. Dudziak, and R. J. LaBauve, "^{6}Li and ^{7}Li Data in the ENDF/B Format," Los Alamos Scientific Laboratory report LA-3695-MS (March 1967).

APPENDIX

CROSS SECTIONS AND CALCULATIONAL COEFFICIENTS

TABLE A-I

ANGULAR-DEPENDENT CROSS SECTIONS

(mb/sr)

Reaction and Neutron Group	Laboratory Angle										
	25°	35°	45°	53°	60°	80°	87°	95°	110°	130°	144°
^{6}Li + 5.96 MeV											
Elastic	473 ± 36	305 ± 23	185 ± 14		74 ± 6	38.3 ± 3.0	35.3 ± 2.5	33.2 ± 2.5	30.6 ± 2.3	29.5 ± 2.2	31.5 ± 2.3
2.18	25 ± 2.5	23.8 ± 2.0	23.9 ± 2.0		20.4 ± 1.7	15.4 ± 1.3	12.2 ± 1.0	11.2 ± 1.0	8.5 ± 0.7	6.1 ± 0.5	5.2 ± 0.5
Continuum	80 ± 10	72 ± 9	72 ± 9		58 ± 8	39 ± 5	32 ± 4	25 ± 3	23 ± 3	22 ± 3	16 ± 2
^{7}Li + 5.96 MeV											
Elastic + 0.48	570 ± 43	392 ± 30	231 ± 18		108 ± 8	64 ± 5	66 ± 5	68 ± 5	67 ± 5	55 ± 4	47 ± 4
4.63	42.6 ± 4.3	31.2 ± 3.6	26.0 ± 4.4		19.9 ± 5						
Continuum		43 ± 6	36 ± 5		24 ± 4	18 ± 3	15 ± 2	16 ± 2	14 ± 2	7 ± 2	10 ± 2
^{6}Li + 9.83 MeV											
Elastic	560 ± 44	324 ± 25	157 ± 12	70 ± 6	48 ± 4	16.6 ± 4		15.4 ± 1.2	15.3 ± 1.2	10.6 ± 0.8	9.4 ± 0.8
2.18			18.6 ± 2.6	15.4 ± 1.8	15.6 ± 2.6	10.8 ± 1.9		5.2 ± 0.9	5.4 ± 0.9	4.3 ± 0.7	3.2 ± 0.7
4.31	19 ± 5	15 ± 4	14 ± 4		7 ± 2	3 ± 1.5		3.5 ± 2.0	3 ± 2	4 ± 2	2 ± 2
Continuum	84 ± 10	77 ± 10	65 ± 10	61 ± 8	50 ± 8	34 ± 5		29 ± 5	20 ± 3	17 ± 3	16 ± 3
^{7}Li + 9.83 MeV											
Elastic + 0.48	568 ± 44	392 ± 30	214 ± 17	98 ± 8	65 ± 5	36.3 ± 2.8		36.2 ± 2.8	32.6 ± 2.6	21.5 ± 1.7	17.5 ± 1.4
4.63	24.0 ± 1.8	18.8 ± 1.3	17.3 ± 1.2	13.8 ± 1.8	17.0 ± 1.2	11 ± 1		8.1 ± 0.6	6.0 ± 0.5	4.4 ± 0.5	3.9 ± 0.5
6.7	5.7 ± 2.5	5.0 ± 2.5	4.4 ± 2.2		3.4 ± 1.7	2.4 ± 1.2		2.1 ± 1.1	1.8 ± 0.9	1.1 ± 0.6	1.0 ± 0.5
Continuum	33 ± 5	33 ± 5	36 ± 5	33 ± 8	26 ± 4	17.2 ± 2.6		16.5 ± 2.5	11.7 ± 1.8		7.0 ± 1.0

TABLE A-II

INTEGRATED CROSS SECTIONS

Reaction and Neutron Group	Cross Section (mb)
^{6}Li + 5.96-MeV Neutrons	
Elastic	1308 ± 82
2.18-MeV State	171 ± 14
Continuum	496 ± 64
^{7}Li + 5.96-MeV Neutrons	
Elastic + 0.48-MeV State	1715 ± 108
4.63-MeV State	127 ± 50
Continuum	249 ± 35
^{6}Li + 9.83-MeV Neutrons	
Elastic	1044 ± 85
2.18-MeV State	121 ± 15
4.31-MeV State[a]	61 ± 30
Continuum	472 ± 60
^{7}Li + 9.83-MeV Neutrons	
Elastic + 0.48-MeV State	1344 ± 107
4.63-MeV State	127 ± 15
6.7-MeV State[a]	32 ± 16
Continuum	235 ± 35

[a]Included in the continuum.

TABLE A-III

DOUBLE-DIFFERENTIAL CONTINUUM CROSS SECTIONS

Reaction and Emergent Neutron Energy Interval (MeV)	(mb/sr) Laboratory Angle									
	25°	35°	45°	60°	80°	87°	95°	110°	130°	144°
^{6}Li + 5.96 MeV										
0.0 – 0.5	16 ± 8	17 ± 8	19 ± 9	16 ± 9	12 ± 6	12 ± 6	9 ± 5	9 ± 5	11 ± 5	5 ± 3
0.5 – 1.0	32 ± 3	35 ± 3	30 ± 3	27 ± 3	22 ± 3	21 ± 3	19 ± 2	17 ± 2	19 ± 2	18 ± 2
1.0 – 1.5	29 ± 3	30 ± 3	24 ± 3	25 ± 3	20 ± 2	16 ± 2	11 ± 1	10 ± 1	9 ± 2	7 ± 1
1.5 – 2.0	26 ± 3	25 ± 3	21 ± 2	20 ± 2	13 ± 2	9 ± 2	6 ± 2	4 ± 2	3 ± 2	2 ± 1
2.0 – 2.5	23 ± 3	14 ± 2	17 ± 2	14 ± 3	7 ± 3	4 ± 2	3 ± 2	1 ± 1	2 ± 1	1 ± 1
2.5 – 3.0	16 ± 2	12 ± 3	16 ± 4	8 ± 4	4 ± 2	2 ± 1	1 ± 1			
3.0 – 3.5	13 ± 4	9 ± 4	12 ± 6	4 ± 2	1 ± 1					
3.5 – 4.0	6 ± 2	2 ± 2	5 ± 3	2 ± 2						
^{7}Li + 5.96 MeV										
0.0 – 0.5		5 ± 3	7 ± 4	6 ± 3	6 ± 3	6 ± 3	6 ± 3	8 ± 4	4 ± 2	6 ± 3
0.5 – 1.0		22 ± 10	12 ± 6	9 ± 5	12 ± 6	9 ± 4	9 ± 3	10 ± 3	6 ± 2	8 ± 2
1.0 – 1.5		22 ± 10	12 ± 4	12 ± 2	8 ± 1	6 ± 1	5 ± 1	4 ± 1	2 ± 0.5	3 ± 0.5
1.5 – 2.0		12 ± 2	12 ± 2	8 ± 1	4 ± 0.5	2 ± 0.5	1 ± 0.5	1 ± 0.5	1 ± 0.5	2 ± 0.5
2.0 – 2.5		7 ± 1	10 ± 1	5 ± 0.5	3 ± 0.5	3 ± 0.5	2 ± 0.5	2 ± 0.5	1 ± 1	2 ± 1
2.5 – 3.0		6 ± 0.5	7 ± 0.5	2 ± 0.5	2 ± 0.5	3 ± 0.5	3 ± 0.5	2 ± 0.5		
3.0 – 3.5		4 ± 0.5	5 ± 0.5	3 ± 0.5	1 ± 1	1 ± 1	1 ± 1	1 ± 1		
3.5 – 4.0		4 ± 1	4 ± 0.5	2 ± 1						
4.0 – 4.5		4 ± 1	3 ± 2							
^{6}Li + 9.83 MeV										
0.0 – 0.5	8 ± 5	8 ± 4	7 ± 4	10 ± 5	9 ± 5	3 ± 2	6 ± 3	4 ± 2	4 ± 2	5 ± 2
0.5 – 1.0	16 ± 3	19 ± 3	14 ± 3	16 ± 3	14 ± 2	10 ± 2	8 ± 2	8 ± 2	7 ± 2	7 ± 2
1.0 – 1.5	16 ± 3	14 ± 3	10 ± 2	13 ± 2	10 ± 2	8 ± 2	7 ± 1	5 ± 1	5 ± 1	6 ± 1
1.5 – 2.0	10 ± 2	10 ± 2	8 ± 1	10 ± 1	8 ± 1	6 ± 1	6 ± 1	5 ± 1	5 ± 1	4 ± 1
2.0 – 2.5	10 ± 1	9 ± 1	8 ± 1	9 ± 1	8 ± 1	6 ± 1	6 ± 1	5 ± 1	5 ± 1	4 ± 1
2.5 – 3.0	8 ± 1	9 ± 1	8 ± 1	9 ± 1	8 ± 1	7 ± 1	6 ± 1	5 ± 1	4 ± 1	2 ± 1
3.0 – 3.5	10 ± 1	9 ± 1	9 ± 1	9 ± 1	8 ± 1	6 ± 1	5 ± 1	4 ± 1	2 ± 1	1 ± 1
3.5 – 4.0	10 ± 1	9 ± 1	9 ± 1	9 ± 1	9 ± 1	7 ± 1	5 ± 1	2 ± 1		
4.0 – 4.5	11 ± 1	10 ± 1	11 ± 1	8 ± 1	10 ± 2	6 ± 1	4 ± 1	1 ± 1		
4.5 – 5.0	12 ± 1	12 ± 1	13 ± 1	8 ± 1	8 ± 2	5 ± 2	2 ± 1			
5.0 – 5.5	16 ± 2	14 ± 2	11 ± 1	8 ± 1	4 ± 2	2 ± 1	2 ± 1			
5.5 – 6.0	12 ± 1	14 ± 2	10 ± 2	7 ± 2	2 ± 1	1 ± 1	1 ± 1			
6.0 – 6.5	10 ± 1	10 ± 3	6 ± 2	4 ± 2	1 ± 1	1 ± 1				
6.5 – 7.0	9 ± 2	7 ± 3	4 ± 2	2 ± 1						
7.0 – 7.5	5 ± 2	3 ± 2	2 ± 1							
7.5 – 8.0	4 ± 2									
8.0 – 8.5	2 ± 1									

TABLE A-III (cont)

Reaction and Emergent Neutron Energy Interval (MeV)	(mb/sr) Laboratory Angle									
	25°	35°	45°	53°	60°	80°	95°	110°	130°	144°
^{7}Li + 9.83 MeV										
0.0 – 0.5	4 ± 2	4 ± 2	6 ± 3	5 ± 2	4 ± 2	2 ± 1	2.5 ± 1	4 ± 2	2.5 ± 1.3	2.± 1
0.5 – 1.0	5.5 ± 1.3	7 ± 1.8	6 ± 1.5	7 ± 3	6 ± 2	5 ± 1.2	4 ± 1	4.6 ± 1.3	3.1 ± 0.9	2.5 ± 0.7
1.0 – 1.5	5 ± 1.1	7 ± 1	7 ± 1	7 ± 2.4	6 ± 0.8	5 ± 0.8	4 ± 0.6	4.4 ± 0.7	2.6 ± 0.8	2.5 ± 0.2
1.5 – 2.0	6 ± 1.4	7 ± 1	8 ± 1	7 ± 2.4	6 ± 0.8	5.8 ± 1	4 ± 0.6	3.6 ± 0.6	2.1 ± 0.5	2.3 ± 0.5
2.0 – 2.5	6 ± 1.4	8 ± 1.1	7 ± 1.1	6 ± 2.1	8 ± 1.1	5.6 ± 0.8	3.4 ± 0.6	3 ± 0.5	1.6 ± 0.5	1 ± 0.6
2.5 – 3.0	9 ± 2	9 ± 1.3	8 ± 1.1	7 ± 2.4	7 ± 1	2.8 ± 0.6	2.5 ± 0.4	2.2 ± 0.6	1.1 ± 0.5	1.1 ± 0.8
3.0 – 3.5	8 ± 1.8	7 ± 1	7 ± 1	6 ± 3.1	5 ± 0.7	2.5 ± 0.5	1.9 ± 0.3	1.2 ± 0.3	0.8 ± 0.5	0.6 ± 0.4
3.5 – 4.0	7 ± 2	6 ± 0.8	6 ± 1	4 ± 1.4	3.5 ± 0.5	1.9 ± 1.0	1.6 ± 0.3	0.9 ± 0.3	0.3 ± 0.2	0.3 ± 0.2
4.0 – 4.5	6 ± 2	5 ± 2	5 ± 1	4 ± 2	2.2 ± 1	2.3 ± 1.0	1.0 ± 0.5	0.8 ± 0.3		
4.5 – 5.0	5 ± 2	5 ± 2	4 ± 1	3 ± 1.5	1.5 ± 0.8	0.9 ± 0.3	0.6 ± 0.5	0.5 ± 0.2		
5.0 – 5.5	2 ± 0.5	4 ± 2	3 ± 0.4	3 ± 1.2	1.2 ± 0.2	0.6 ± 0.2	0.9 ± 0.2			
5.5 – 6.0	3 ± 0.7	4 ± 0.6	3 ± 0.4	2.5 ± 1.2	1.2 ± 0.2	0.6 ± 0.2	0.8 ± 0.1			
6.0 – 6.5	1 ± 1	4 ± 0.6	2 ± 0.3	1.6 ± 0.6	0.6 ± 0.2		0.5 ± 9.1			
6.5 – 7.0	1 ± 1	3 ± 0.4	3 ± 0.4	2.5 ± 0.4						
7.0 – 7.5		2 ± 1	2 ± 0.3	1.2 ± 0.5						
7.5 – 8.0		1 ± 1	1 ± 0.5							

TABLE A-IV

CENTER-OF-MASS LEGENDRE POLYNOMIAL COEFFICIENTS FOR ELASTICALLY SCATTERED NEUTRONS

Reaction	A_0	A_1	A_2	A_3	A_4	A_5
^{6}Li + 5.96-MeV Neutrons	98 ± 2	146 ± 3	155 ± 4	100 ± 4	47 ± 5	19 ± 5
^{7}Li + 5.96-MeV Neutrons	140 ± 9	173 ±16	190 ± 25	123 ± 31	33 ± 35	−28 ± 33
^{6}Li + 9.83-MeV Neutrons	94 ± 13	181 ± 21	169 ± 31	114 ± 39	60 ± 50	26 ±41
^{7}Li + 9.83-MeV Neutrons	108 ± 7	191 ± 11	197 ± 18	153 ± 22	64 ± 27	14 ± 23

Printed in the United States of America
Available from
National Technical Information Service
US Department of Commerce
5285 Port Royal Road
Springfield, VA 22161

Microfiche $3.50 (A01)

Page Range	Domestic Price	NTIS Price Code	Page Range	Domestic Price	NTIS Price Code	Page Range	Domestic Price	NTIS Price Code	Page Range	Domestic Price	NTIS Price Code
001-025	$ 5.00	A02	151-175	$11.00	A08	301-325	$17.00	A14	451-475	$23.00	A20
026-050	6.00	A03	176-200	12.00	A09	326-350	18.00	A15	476-500	24.00	A21
051-075	7.00	A04	201-225	13.00	A10	351-375	19.00	A16	501-525	25.00	A22
076-100	8.00	A05	226-250	14.00	A11	376-400	20.00	A17	526-550	26.00	A23
101-125	9.00	A06	251-275	15.00	A12	401-425	21.00	A18	551-575	27.00	A24
126-150	10.00	A07	276-300	16.00	A13	426-450	22.00	A19	576-600	28.00	A25
									601-up	†	A99

†Add $1.00 for each additional 25-page increment or portion thereof from 601 pages up.